

See discussions, stats, and author profiles for this publication at: <https://www.researchgate.net/publication/356639589>

Prediction and analysis of the cavitating performance of a Francis turbine under different loads

Article in *Energy Sources, Part A: Recovery, Utilization and Environmental Effects* · November 2021

DOI: 10.1080/15567036.2021.2009941

CITATIONS

0

READS

59

4 authors, including:



Ali Abbas

Flovel Energy pvt ltd

9 PUBLICATIONS 19 CITATIONS

[SEE PROFILE](#)



Md. Mustafa Kamal

Indian Institute of Technology Roorkee

3 PUBLICATIONS 1 CITATION

[SEE PROFILE](#)



Gaurav Saini

Indian Institute of Engineering Science and Technology, Shibpur

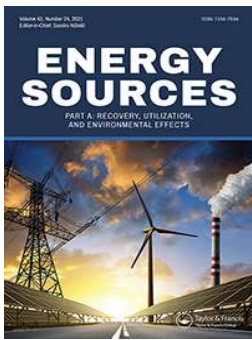
16 PUBLICATIONS 87 CITATIONS

[SEE PROFILE](#)

Some of the authors of this publication are also working on these related projects:



Development of an efficient hydro kinetic turbines [View project](#)



Prediction and analysis of the cavitating performance of a Francis turbine under different loads

Md. Mustafa Kamal, Gaurav Saini, Ali Abbas & Vishnu Prasad

To cite this article: Md. Mustafa Kamal, Gaurav Saini, Ali Abbas & Vishnu Prasad (2021): Prediction and analysis of the cavitating performance of a Francis turbine under different loads, Energy Sources, Part A: Recovery, Utilization, and Environmental Effects, DOI: [10.1080/15567036.2021.2009941](https://doi.org/10.1080/15567036.2021.2009941)

To link to this article: <https://doi.org/10.1080/15567036.2021.2009941>



Published online: 30 Nov 2021.



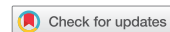
Submit your article to this journal [↗](#)



View related articles [↗](#)



View Crossmark data [↗](#)



Prediction and analysis of the cavitating performance of a Francis turbine under different loads

Md. Mustafa Kamal^a, Gaurav Saini^b, Ali Abbas^c, and Vishnu Prasad^d

^aDepartment of Hydro and Renewable Energy, Indian Institute of Technology Roorkee, Roorkee, India; ^bSchool of Advanced Materials, Green Energy and Sensor Systems, Indian Institute of Engineering Science and Technology, Shibpur, India; ^cDepartment of Mechanical Engineering, Madanapalle Institute of Technology & Science, Madanapalle, India; ^dDepartment of Civil Engineering, Maulana Azad National Institute of Technology, Bhopal, India

ABSTRACT

The variations in the operating conditions of Francis turbines may lead to cavitation due to pressure pulsations in vanless space. In order to combat the fluctuations in power demand and input flow conditions such as net head and discharge, the turbine needs to be operated at off-design conditions. Due to the higher demand of medium-specific speed Francis turbine at most of the hydropower plants, it is necessary to predict the low-pressure zone and vapor bubbles formation on the surface of turbine runner blades. Under the present study, it is proposed to investigate the cavitation and performance characteristics of a medium-specific speed Francis turbine. In order to resemble the fluctuations in load, three different operating regimes, i.e. part-load, rated load and over-load, were considered to especially highlight the performance under cavitation and without cavitation conditions of the turbine. Based on investigations, it has been revealed that turbine experiences a minimum drop in hydraulic efficiency corresponding to rated-load operation and the maximum drop in efficiency was observed during the over-load operation. The pressure variations across the runner blades were observed at mid-span of the blade in stream-wise direction. The cavitation characteristics of the turbine were derived by using the sigma curve and the vapor volume fraction. The critical values of sigma for part-load, rated-load, and over-load regimes were obtained as 0.18, 0.12, and 0.16, respectively. The results obtained under the present investigation were verified by the experimental model testing results of the turbine.

ARTICLE HISTORY

Received 24 February 2021
Revised 12 November 2021
Accepted 15 November 2021

KEYWORDS

Renewable energy;
hydropower; Francis Turbine;
cavitation; hydraulic
efficiency

Introduction

Hydropower played a crucial role in the economic development of many countries (Saini and Saini 2019). This promising technology ensures the least environmental impact among other renewable resources (Kamal 2017). In order to tap the hydropower energy with conventional manner, mainly two types of turbine have been employed like impulse (Pelton, Turgo-impulse) and Reaction (Francis and Kaplan turbine) (Jain 2002). Francis turbine gained more popularity among other conventional turbines due to its maximum efficiency among available conventional hydro turbines (IHA 2020). Therefore, this turbine is always designed to operate at best efficiency point (BEP) condition (Celebioglu et al. 2017),(Celebioglu et al., 2018). In reality, it is quite impossible to run a turbine at rated condition due to load variations caused by variations in input parameters (head and discharge) and output parameters (power and RPM). It leads to various unsteady phenomenon such as pressure pulsation in draft tube, vortex rope formation at the outlet of runner, and cavitation occurrence on the

surface of runner blade. (Trivedi, Gandhi, and Michel 2013). The hydraulic efficiency of turbine is greatly affected by these unsteady phenomena. The hydraulic efficiency of a hydraulic turbine can mathematically be expressed as;

$$\text{Hydraulic efficiency}(\eta_H) = \frac{P_o}{P_i} = \frac{T\omega}{(p_{inlet} - p_{outlet})Q} \quad (1)$$

Where P_o is the output power and P_i is the input power. T and ω are the torque and angular speed of the turbine shaft. Q is the discharge and p_{inlet} and p_{outlet} are the total inlet and outlet pressure.

Cavitation is a phenomenon in which growth of bubbles take place when local pressure of liquid reduces to its vapor pressure at constant temperature and collapse at high pressure zone when compressive force act on these bubbles (Huang, Wu, and Wang 2014). It is also known as cold boiling process. Cold boiling is different from conventional boiling because phase change takes place due to reduction in local pressure while local temperature increases in boiling (Jean et al. 2004a).

Cavitation may occur in every reaction turbine. Zhang et al. (2018) analyzed the effects of cavitation on blade design. In Francis turbine, cavitation are more prone under high and medium specific speed turbine than low specific speed turbine due to high velocity of flowing fluid. Major cavitation occurrences are leading edge cavitation, trailing edge cavitation, inter-blade vortex cavitation, vortex rope cavitation, and Von-Karman vortex cavitation (Jean et al., 2004a).

Cavitation in hydro turbine is usually assessed by 'Cavitation number', which is suggested by Prof. Dietrich Thomas (Jean et al., 2004b). Cavitation number (σ_{plant}) is used to determine the specific zone where turbine can work without being affected from cavitation (Lal 2011). Cavitation number is directly related to the turbine characteristics and its installation setting at the site. Cavitation cannot always be nullified but it can be minimized by adjusting the setting of turbine above or below the tail race level, proper design of runner blades, and limit the off-design operating points. To achieve the cavitation-free operation, plant sigma should be greater than turbine sigma at all the operating points. Plant sigma and turbine sigma can be evaluated by the following expression;

$$\sigma_{plant} = \frac{\left(\frac{P_a - P_v}{\rho g}\right) - H_s}{H_n} \quad (2)$$

$$\sigma_{turb} = \frac{\left(\frac{P_a - P_i}{\rho g}\right) - H_s}{H_n} \quad (3)$$

Where, P_a and P_v is ambient and vapor pressure of fluid, respectively. P_i is absolute static pressure of flowing fluid at any point in flow domain. H_s is suction head or turbine setting level above tail race. H_n is the working head or net head of turbine.

To visualize the bubbles formation on blade surface and draft tube, various authors have carried out experimental studies and derived the cavitation characteristics of hydro turbine. However, experimentation work has different limitations, i.e. applicable for limited operating points, requires highly accurate and precise instrumentation. To subdue this, a Computational Fluid Dynamics (CFD) tool became a 'virtual laboratory' to many researchers for conducting the unsteady flow analysis of hydro turbine (Liu et al. 2015).

CFD is basically a prediction tool which predicts the behavior of flow in specified flow domain (Versteeg and Malalasekera 2007). That is why it requires a validation with experimental data. It plays a significant role to investigators/researchers to understand the flow behavior at each operating point, which is not feasible with experimental one. Based on the requirement, steady and unsteady analysis are generally carried out by using the Reynolds-averaged Navier-Stoke equations (RANS) and Unsteady Reynolds-averaged Navier-Stoke equations (URANS), respectively. Lot of investigations have been carried out to understand the scope of CFD for the prediction of cavitation in hydro turbine and are summarized in Table 1.

Table 1. Summary of the numerical investigations on hydro turbine.

Author	Cavitation model	Solver code	Objectives	Findings/Remarks
Chirkov et al. (2019)	In-house model	In-house solver code	To evaluate the instability and pressure pulsation induced in Francis turbine at full load condition	A novel hybrid model has been established in which 1D hydro-acoustic equation was used to evaluate the flow behavior in penstock and 3D Navier-Stoke equation for the turbine domain.
Yang, Zhou, and Wang (2019)	Zwart-Gerber-Belamri	—	To derive the oscillating characteristics of flow in Francis turbine under full load operation	It was observed that the loading conditions have significant effects on average volume of vortex rope.
Yamamoto et al. (2019)	Rayleigh-Plesset equation	CFX	To observe the mechanism of inter-blade cavitation in Francis turbine under part-load condition.	A recirculating flow near hub at the blade outlet has been observed, which further participated in the development of inter-blade cavitation.
Zhang et al. (2019)	—	—	To optimize the turbine impeller under cavitation condition	It was concluded that the impeller showed poor cavitation characteristics under part-load condition due to the flow separation at the rear side of impeller. The impeller shape was optimized by increasing the inlet receiving angle by 5°.
Tiwari et al. (2020b)	Rayleigh-Plesset	CFX	To determine the cavitation characteristics of Francis turbine	It was reported that the turbine is more subjected to runner core cavitation while operating at part-load regime. Also, the overall damage due to cavitation was observed at over-load condition.
Sun, Guo, and Luo (2020)	Zward model	CFX	To predict the inter-blade cavitation structure in Francis turbine.	A helical shaped vortex core was observed at the outlet of runner.
Trivedi et al. (2020)	Rayleigh-Plesset	CFX	To study the inception of cavitation in Francis turbine at variable speeds.	The cavitation was found maximum at higher value of rotational speed. The cavitation was observed at the guide vanes and stay vanes passage and at the trailing edge of runner blades.
Celebioglu et al. (2017)	—	CFX	To study the cavitation characteristics of Francis turbine	Blade was redesigned to provide cavitation free operation and also determined cavitation limit for off-design operating conditions.
Decaix et al. (2015)	Rayleigh-Plesset	CFX	Validation of cavitating vortex rope at full load condition using homogeneous RANS model.	The global performance of turbine was under-estimated as compared to experimental results.
Gohil and Saini (2015)	Rayleigh-Plesset	CFX	Effect of suction head, temperature and velocity on cavitation in a Francis turbine.	Efficiency loss and cavitation increases with suction head and temperature. Efficiency loss decreased initially and attained minima then increased with the flow velocity.
Gohil and Saini (2016)	Rayleigh-Plesset	CFX	Effect of variable operating load conditions were evaluated on Francis turbine of small hydro plant in terms of efficiency, volume fraction of water vapor.	Efficiency loss was observed minimum at rated load and maximum at overload operating condition. Volume fraction of water vapor was maximum under overload condition.
Laouari and Ghenaïet (2016)	Rayleigh-Plesset	CFX	Turbine efficiency was analyzed under different cavitation number and off designed conditions were investigated.	Hydraulic efficiency was more affected by cavitation number. Efficiency loss increased with suction head. Cavitation number was found least at BEP than off-design point.
Su et al. (2013)	LES	—	To understand the flow characteristics at off-design point with single-phase and two-phase model.	Channel vortices, vortex rope, and pressure pulsation in draft tube were predicted with better accuracy by using two-phase model than single-phase model.

(Continued)

Table 1. (Continued).

Author	Cavitation model	Solver code	Objectives	Findings/Remarks
Wack et al. (2015)	–	CFX	Prediction of cavitation phenomenon in a Francis turbine at deep part load condition.	Inter-blade vortices have been observed at the runner blade.
Wack et al. (2017)	–	CFX	Vortex rope generation at part load condition was analyzed at different cavitation number.	Vapor volume fraction was found to be increased with reduction in pressure level. Amplitude of pressure fluctuation decreased with reduction of cavitation number.
Wei et al. (2014)	Rayleigh-Plesset	CFX	To determine the effect of perforation on cavitation characteristics of turbine.	Perforation has no influence on critical cavitation and efficiency but it reduces the cavitation area. Shape of vortex rope at the inlet of draft tube changed and also high frequency bubbles were disappeared. Due to perforation, amplitude of pressure pulsations were highly reduced.
Yu, Luo, and Ji (2015)	–	–	To study the effect of air admission in Francis turbine on vorticity.	Aeration depressed the vertical flow and minimized pressure pulsation in draft tube with suitable air volume fraction.
Zhang et al. (2018)	SST	Open-foam	Cavitating flow in high head Francis turbine at part load condition using open-foam was investigated.	Results from simulation, which is volume fraction of water vapor on blade had good agreement with eroded prototype runner.

Lot of investigations have been carried out to predict the cavitation characteristics for low and high specific speed Francis turbine. Based on the investigations, it has been observed that the medium specific speed-based Francis runner has not been extensively studied to predict the cavitation characteristics. Simultaneously, the flow visualizations across the runner blades have also not been covered in earlier investigations. By keeping in view the aforementioned issues and to understand the wide applicability of medium speed Francis turbine runner, the present study is aimed to investigate the cavitation, progression characteristics of water vapors on blade surface, and the vortex formation around runner blades of Francis turbine. A cavitating flow analysis was carried out on scaled down model of actual medium specific speed mixed-flow Francis turbine having rated power of 281 MW, operating under 86 m of rated head and 253 specific speed. Simulations were carried out under the three different loading regimes i.e., part-load (51% of rated-load), rated-load, and over-load (127% of rated-load) conditions. Variations in loading conditions were made by adjusting the guide vanes opening (GVO). The details of considered design and flow parameters for mixed flow medium specific speed Francis turbine are given in [Table 2](#).

Table 2. Design and flow parameters for Francis turbine model.

Parameters	Value/Range
Runner diameter (m)	0.4
No. of runner blades (-)	13
No. of guide vanes (-)	24
No. of stay vanes (-)	24
Head (m)	20
Range of GVO (°)	14.01°–34°
Blade inlet angle (°)	35.74°
Blade outlet angle (°)	24.36°
Discharge (lps)	343.46–840.76

Simulation methodology

In this section, CAD software has been used to develop the 3D model of Francis turbine and mesh properties have been discussed. Selection of turbulence model and cavitation model have also been elaborated. The details of operating points and boundary conditions for CFD simulation have been summarized.

3D modeling and grid generation

3D modeling of all the components have been done in ‘Solid works’ and ‘ANSYS Design modeler’ based on drawing. The profile of runner blade is created by using the ‘BladeGen’ module. Surfacing is done in solid works as per design parameter and further is converted into solid body by using design modeler. The complete CFD domain consists of spiral casing, stay vanes (SV), guide vanes (GV), runner, and draft tube. The complete domain was divided into two sub-domains, i.e., stationary domain (spiral casing, SV, GV, and draft tube) and rotating domain (runner). The complete 3D scaled model of Francis turbine is presented in [Figure 1](#).

Domain discretization can be done mainly by two ways, i.e., spatial discretization and temporal discretization. In spatial discretization, the physical space where flow is taking place is divided into different small cells, termed as grid cell, and the process is known as grid generation. Then these numerical approximations are employed on these discrete points, the so-called grid points. Accuracy of the results depends on density of elements within the flow domain, but over dense elements may

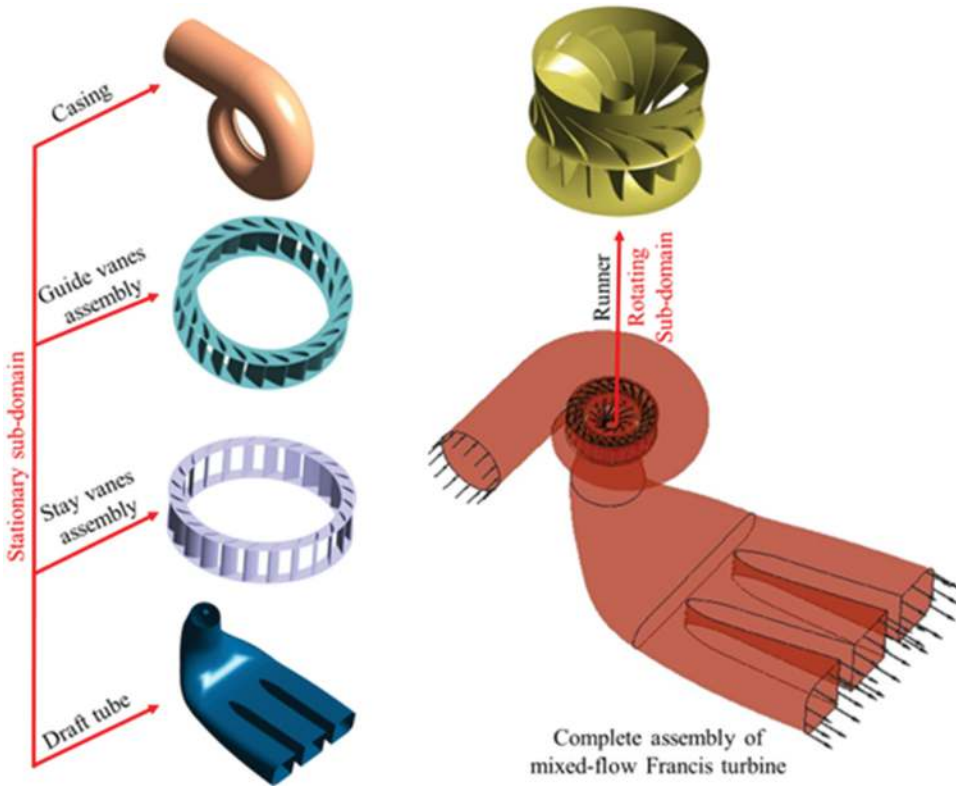


Figure 1. 3D scaled model of Francis turbine.

result in enhanced computational cost. In order to effectively capture the flow field, the complex and critical regions (edges and curvatures) were given fine mesh, and the coarse mesh elements were adopted for simple and less critical regions.

In the present study, 'ICEM and ANSYS Mesh' module have been used for grid generation. A hybrid-mesh type was adopted for grid generation. Casing, stay vanes, guide vanes, and draft tube were discretized with structured mesh and un-structured type mesh is adopted for the Francis runner. The 'Hexahedral and tetrahedral' element type grid elements have been selected for grid generation. For structured mesh generation, 'ICEM' module has been adopted, while for unstructured mesh generation, 'ANSYS Mesh' module was used. The blocking and meshing of different components of Francis turbine is shown in [Figures 2 and 3](#), respectively.

The convergence of a numerical solution significantly depends on the quality of mesh (Saini and Saini 2020a). Various critical mesh parameters such as maximum skewness, minimum element quality, minimum orthogonal angle, and maximum aspect ratio have been monitored (Wei et al. 2014), which are significant to define the quality of mesh; the mesh quality of different components is described in [Table 3](#). In order to capture the boundary layer phenomenon around the runner blade region, a total of 15 layer of inflation with a first layer thickness value of 0.1 mm has been specified on the surface of blade (Saini and Saini 2020b). The average calculated value of y^+ was obtained as 8.783. The details of mesh generation parameters are summarized in [Table 4](#).

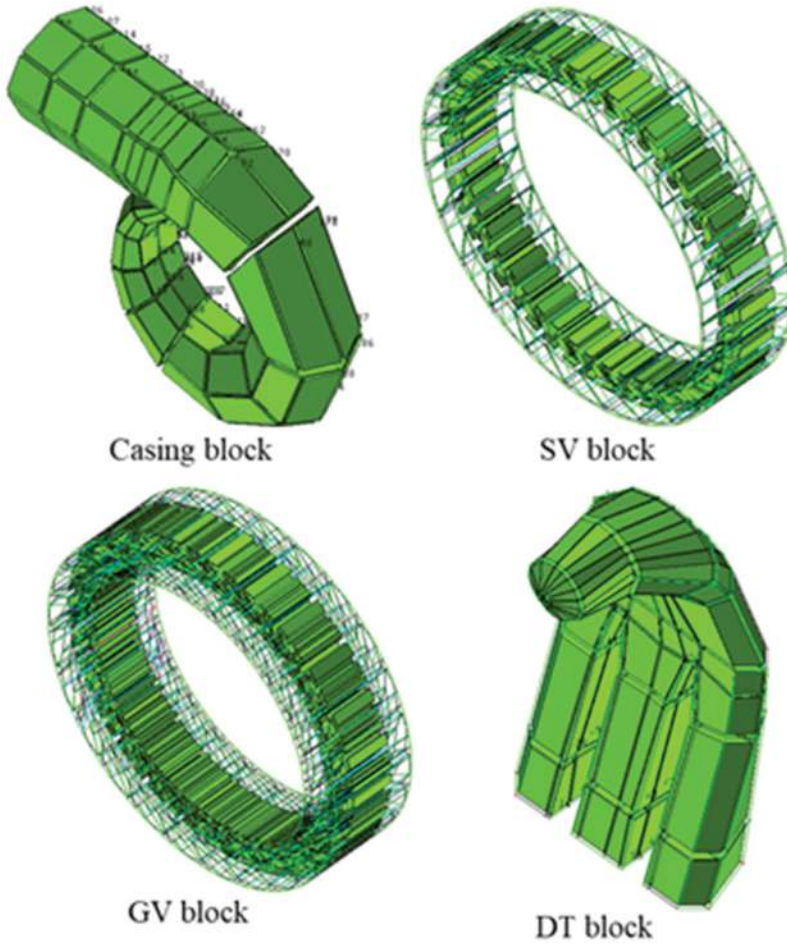


Figure 2. Blocking of different components of the Francis turbine.

Turbulence and cavitation modeling

In this study, SST turbulence model has been used (Kamal et al. 2021), which is proposed by ‘Menter.’ SST turbulence model combines the features of $k-\epsilon$ and $k-\omega$ models. Under the present study, SST model is selected because this improves the accuracy of prediction of flow under strong adverse pressure gradient and boundary layer separation (Menter 1994). SST model can be expressed by the following equation:

$$\mu_t = \frac{a_1 \rho k}{\text{Max.}(a_1 \omega, S f_2)} \quad (4)$$

Where f_2 is a blending function, which is used to achieve a smooth transition between two models and s is shear stress or strain rate.

Cavitation modeling uses volume or mass fraction transport equation to model the liquid-vapor phase change. Mass transfer rate due to phase change can be governed by liquid volume fraction transport equation, which assumes that non-condensable gas phase is well mixed with liquid phase (Blazek 2001), and it can be expressed as:

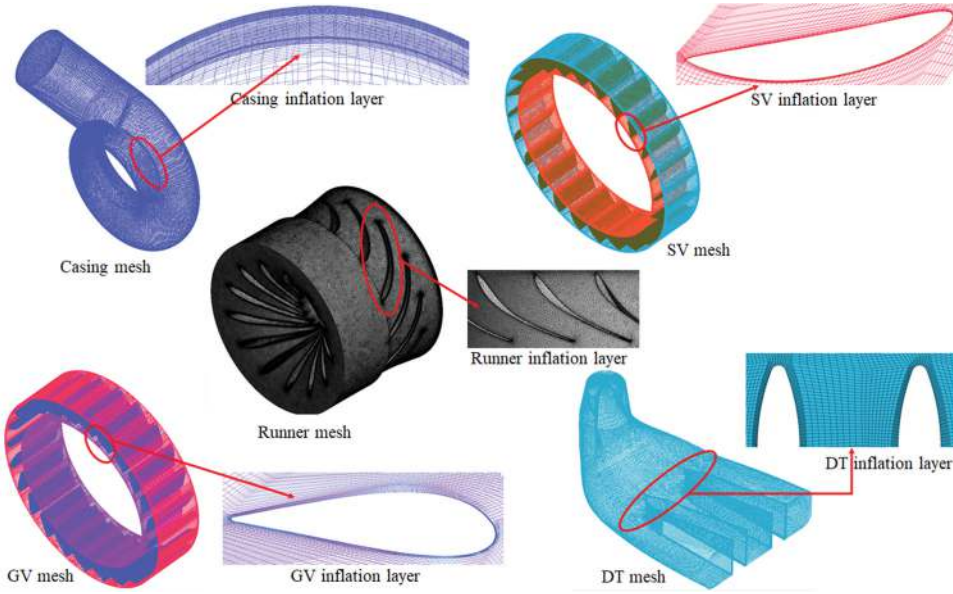


Figure 3. Meshing of different components of the Francis turbine.

Table 3. The details of mesh quality for various components of Francis turbine.

Mesh quality	Casing	Stay vanes	Guide vanes	Runner	Draft tube
Minimum element quality	0.2525	0.2856	0.2894	0.3017	0.2783
Maximum skewness	-	-	-	0.8586	-
Maximum aspect ratio	73	79	81	92	89
Minimum orthogonal angle	23.12	21.76	22.09	-	20.43

Table 4. The details of mesh parameters for various components of Francis turbine.

Components	Number of blocks	Number of nodes	Mesh type	Element type
Spiral casing	216	586,966	Structured	Hexahedral
Stay vanes (SV)	288	356,257	Structured	Hexahedral
Guide vanes (GV)	410	689,356	Structured	Hexahedral
Runner wheel	-	3,526,981	Unstructured	Tetrahedral
Draft tube	123	863,249	Structured	Hexahedral

$$\frac{\partial(\alpha_l \rho_l)}{\partial t} + \frac{\partial(\alpha_l \rho_l V_j)}{\partial X_j} = \dot{m}_l^v - \dot{m}_l^c \quad (5)$$

Where \dot{m}_l^v & \dot{m}_l^c are the mass transfer rate associated with vaporization and condensation, respectively.

In this work, cavitation model based on Rayleigh-Plesset equation is used to estimate the rate of vapor production, i.e. growth of gas bubbles in liquid phase. In order to derive this equation, dynamic viscosity and density of liquid are assumed constant and the pressure within the spherical gas bubble is taken to be uniform. It was also assumed that the bubble will keep its spherical shape in growth as well as collapse (Ramirez et al. 2003) (Ghahramani, Arabnejad, and Bensow 2019). Therefore, the dynamic of a bubble can be described by the following equation (Chang et al. 2017);

$$\frac{p_B(t) - p_\infty(t)}{\rho_l} = R \frac{d^2R}{dt^2} + \frac{3}{2} \left(\frac{dR}{dt} \right)^2 + \frac{4\mu_l}{\rho_l R} \frac{dR}{dt} + \frac{2S}{\rho_l R} \quad (6)$$

Where R is radius of spherical bubble, S represents the surface tension of liquid, ρ_l is the density of liquid, and μ_l is the viscosity of liquid.

The mass transfer rate associated with condensation and vaporization during phase change can be expressed as:

$$\begin{aligned} \dot{m}_l^v &= -F^v \frac{3\alpha_l \alpha_{nuc} \rho_v}{R} \sqrt{\frac{2}{3} \frac{p_v - p_\infty}{\rho_l}} & \text{if } p_\infty < p_v \\ \dot{m}_l^c &= -F^c \frac{3(1 - \alpha_l) \rho_v}{R} \sqrt{\frac{2}{3} \frac{p_\infty - p_v}{\rho_l}} & \text{if } p_\infty > p_v \end{aligned} \quad (7)$$

Where p_v is a vapor pressure of liquid, α_{nuc} is a volume fraction at nucleation site, F is an empirical constant to take into account for the constraint in condensation and vaporization.

Operating points and boundary conditions

In present study, simulations were carried out at three different operating points, i.e. #OP1 Part-load ($\alpha = 14.01^\circ$), #OP2 rated-load ($\alpha = 25.47^\circ$), and #OP3 over-load ($\alpha = 34^\circ$). The details of operating points considered for CFD simulation are given in Table 5.

To solve the algebraic form of CFD governing equations, boundary conditions need to be specified to the domain. Mass flow rate has been given at the inlet of casing, which mimics the water velocity inside the penstock, and a pressure outlet has been specified at the outlet of draft tube. The mass flow rate was computed from specific flow rate, which is expressed by Equation 8. In order to perform the cavitation analysis using ANSYS CFX v18.1, the value of mean diameter of vapor bubbles and interface length scale between liquid and vapor phase are considered as 0.000002 mm and 1.0 mm, respectively. The details of boundary conditions under single phase and two-phase flow conditions are given by Tables 6 and 7, respectively.

$$Q_{11} = \frac{Q}{D^2 \sqrt{H}} \quad (8)$$

Grid independency test

The 'Grid refinement' method is used for mesh-independent results. Four different mesh densities were considered to find the optimized mesh. The mesh independency test is carried out at best efficiency point (BEP). Hydraulic efficiency, net head, and power output were found as the sensitive parameters for mesh independency test. These parameters were selected based on their acceptance on the global parameters for all types of hydro turbines. The number of nodes were varied as 4199715, 4965211, 5543548, 6022809, and 6439871. The minimum numerical errors were obtained as 0.01%, 0.13%, and 0.12%, respectively, corresponding to efficiency, power output, and net head in case of mesh density

Table 5. Details of the operating conditions.

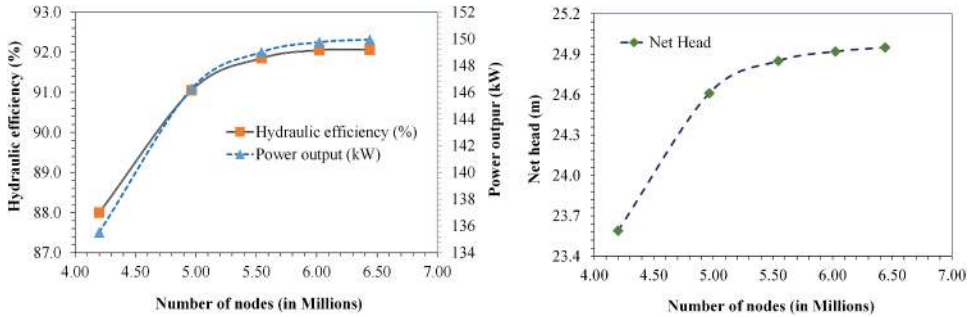
Parameter	#OP1 (At part load)	#OP2 (At BEP)	#OP3 (At over load)
N_{11} (rpm)	75	75	75
Q_{11} (l/s)	480	930	1175
H (m)	20	20	20
GVA ($^\circ$)	14.01	25.47	34

Table 6. Details of boundary condition for single-phase flow simulation.

#OP (Loading condition)	Inlet condition (Mass flow rate, kg/s)	Outlet condition (Average static pressure, Pa)
#OP1. Part-load ($\alpha = 14.01^\circ$)	343.46	101325
#OP2. Rated-load ($\alpha = 25.47^\circ$)	665.49	
#OP3. Over-load ($\alpha = 34^\circ$)	840.76	

Table 7. Details of boundary condition for two-phase flow simulation.

#OP (Loading condition)	Inlet condition (Mass flow rate, kg/s)	Outlet condition (Average static pressure, kPa)
#OP1. Part-load ($\alpha = 14.01^\circ$)	343.46	90,80,70,60,50,40,30,20,10
#OP2. Rated-load ($\alpha = 25.47^\circ$)	665.49	90,80,70,60,50,40,30,20,10
#OP3. Over-load ($\alpha = 34^\circ$)	840.76	90,80,70,60,50,40,30,20,10

**Figure 4.** Variations in hydraulic efficiency, head, and power output corresponding to different mesh counts.

having 6022809 nodes. Hence, the mesh density of 6022809 nodes is considered for all the CFD simulations. The variations of hydraulic efficiency, net head, and power output of turbine with respect to the variations in mesh size refinement are shown in Figure 4.

Based on the analysis, it has been observed that turbine efficiency, net head, and power output increase with mesh density. It is found that the minimum error in the hydraulic efficiency, net head, and power output of turbine is achieved for the mesh density of 6022809 nodes. Further increase in mesh density shows very little variations in output parameters.

Results and discussions

An extensive cavitating study has been carried out on a medium specific speed Francis turbine. The work of post-processing is arranged into three sections. In the first section, mesh independency limit has been performed and validation of numerical simulation with experimental results has been carried out. In the second section, hydrodynamic behavior of Francis runner with and without cavitation has been discussed. In the last section, the cavitation characteristics of considered turbine has been derived.

An attempt has been made to decide the simulation strategy for the present study, and steady and transient-based simulations were performed under the similar operating conditions.

In case of transient analysis, the time step was selected corresponding to 1° of turbine rotation, and a total of five revolutions were considered for each simulation case. It states that the turbine needs to complete 1800 time steps for each transient simulation. To compute the turbine efficiency, average value of the last revolution (5th revolution) has been considered. The maximum deviation in transient and steady state hydraulic efficiency was observed at part-load conditions,

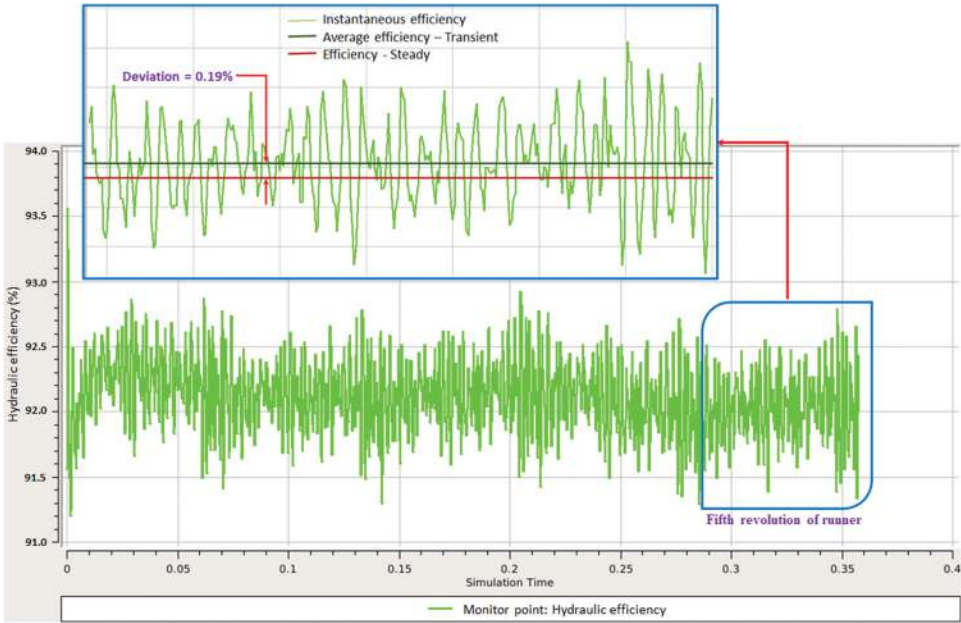


Figure 5. Transient and steady state simulations at rated-load condition.

and minimum deviation was obtained at rated-load condition. The deviation in the hydraulic efficiency under transient and steady state conditions was found as 3.86%, 0.239%, and 0.988%, corresponding to part-load, rated-load, and over-load conditions. A chart for transient and steady state hydraulic efficiency along with deviation at rated-load condition is shown in Figure 5. In addition to this, the variations in hydraulic efficiency, net head, and torque under part-load, rated-load, and over-load conditions are presented in Figure 6. The hydraulic efficiency computed from steady and transient simulation were found as 91.88% and 92.106%, respectively. Based on the comparative analysis, it has been concluded that the deviation in hydraulic efficiency is merely 0.239%, which is in the acceptable level. Therefore, the 'steady-state' approach is adopted for the present study.

Validation of CFD result

Validation is the most important step in order to obtain the authenticity of the results. It is an essential step in numerical investigations to understand the uncertainty of simulations results. In the present study, validation is carried out at best efficiency point (BEP). It has been found that difference between the hydraulic efficiency obtained from numerical and model testing is about $\pm 1.7\%$. The difference between the hydraulic efficiency lies within the maximum experimental uncertainty limit and the numerical errors by considering the simplifications made during the simulations approach. The present validation shows the good agreement of the numerical results with experiments, and computed hydraulic efficiency is on the similar lines with the experimental efficiency. Furthermore, it has also been found that the variations in numerical and experimental work are considerably high at off-design conditions as shown in Figure 7. This is caused by the transient behavior of fluid inside the turbine runner under off-design conditions.

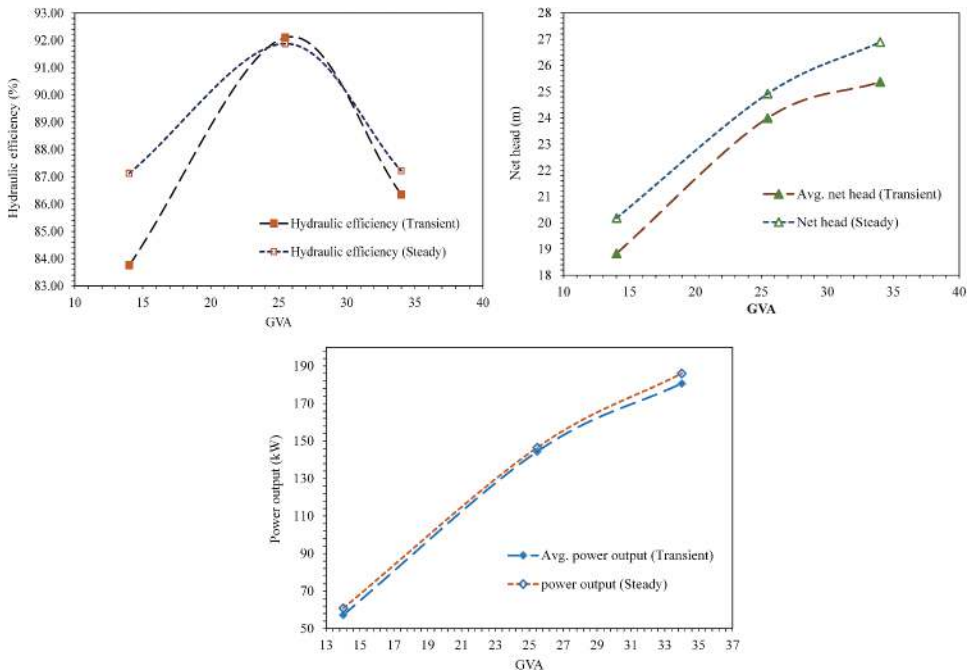


Figure 6. Variations of various output parameters at different loading conditions under steady and transient state simulations.

Hydrodynamic performance of Francis turbine

In this section, the effect of cavitation on hydraulic efficiency, net head, and power output by runner of hydro turbine have been discussed. Also, the pressure pulsation on the runner blade surface has been explored.

Effect of cavitation on performance characteristics of turbine

The hydraulic efficiency of turbine is computed by using Equation (1). The occurrence of cavitation in runner part or draft tube causes reduction in hydraulic efficiency. During cavitation, bubbles formation started, which resists interaction of water with the runner blades. This resisting force reduces the reaction force exerted by the fluid on runner blades and hence reduction in hydraulic efficiency.

The minimum drop in efficiency was observed at BEP condition, while the maximum drop was observed at over-load condition. This is due to the fact that at over-load condition, the velocity carried by water is very high, which results in the reduction of blade water interaction. The comparison of hydraulic efficiency, net head, and power output corresponding to with and without cavitation characteristics were obtained and shown in Figures 8–10. Furthermore, the effect of cavitation on net head and power output has been assessed.

Pressure pulsation on runner blades

The pressure pulsation with and without cavitation on the surface of runner blade has been determined by blade loading curve at mid span of blade in stream-wise direction from leading edge to trailing edge of blade. The static pressure at any point on the mid span of blade is computed in term of pressure coefficient (C_p) by using the Equation (9), and the graphical presentation of the same is shown in Figures 11–13. It was observed that the pressure of fluid decreases from the leading edge to trailing edge due to harness of energy by blade from water. The maximum pressure was observed at the leading edge of pressure side of blade while minimum at the trailing edge of suction side.

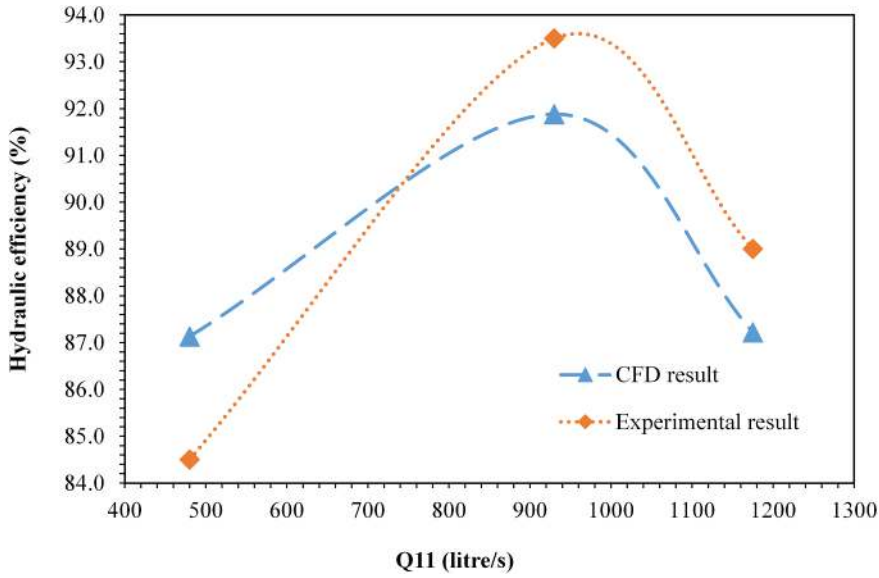


Figure 7. Validation of CFD result with experimental results.

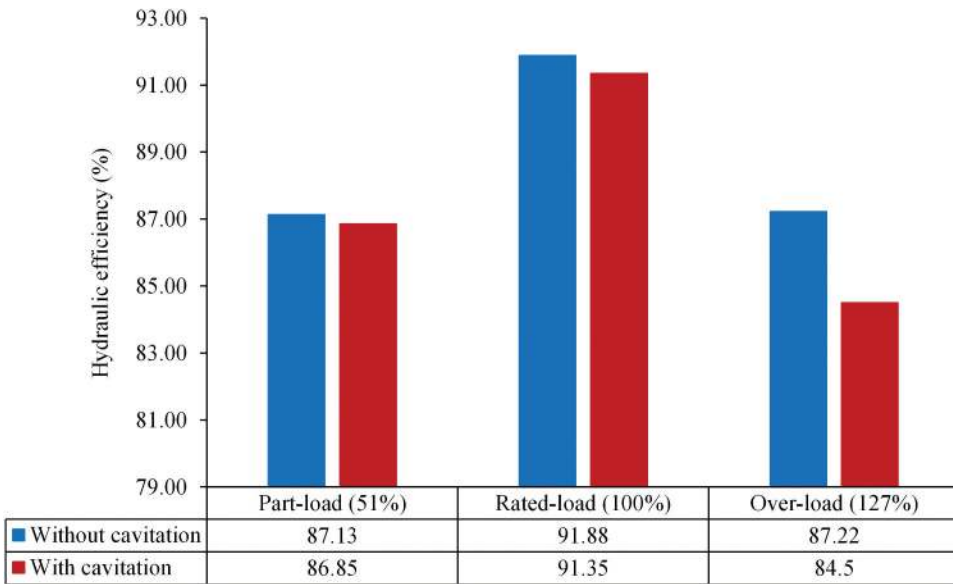


Figure 8. Hydraulic efficiency with and without cavitation at different loading conditions.

$$C_p = \frac{p_i - p_2}{0.5\rho_l W_2^2} \quad (9)$$

The static pressure at any point on the blade surface with cavitation was found lower than the case of without cavitation. This is due to the fact that the flow conditions become more adverse due to the resistance offered by the bubble cavities at developed stage, which causes the formation of small vortices in flowing fluid and leads to high pressure pulsation. The maximum pressure variations across

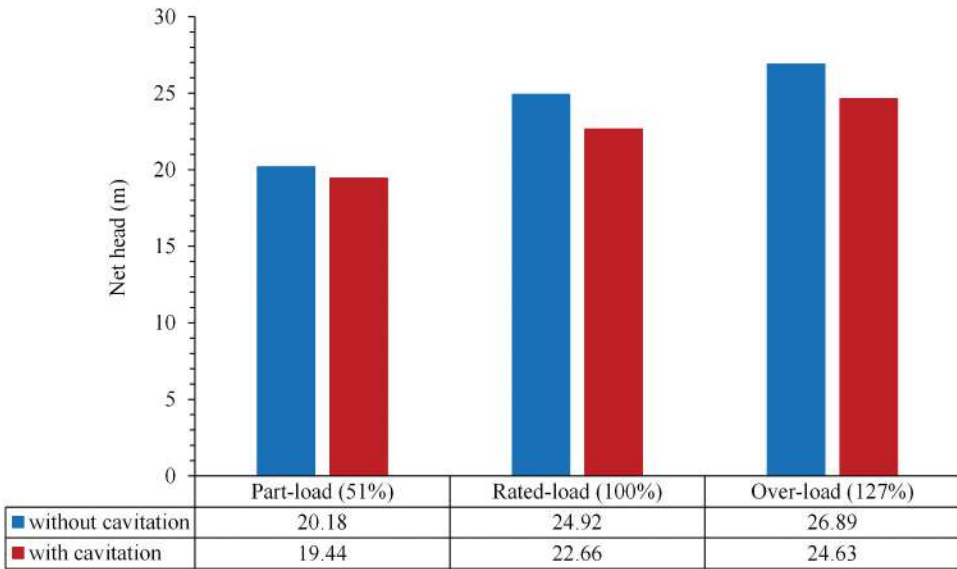


Figure 9. Net head with and without cavitation at different loading conditions.

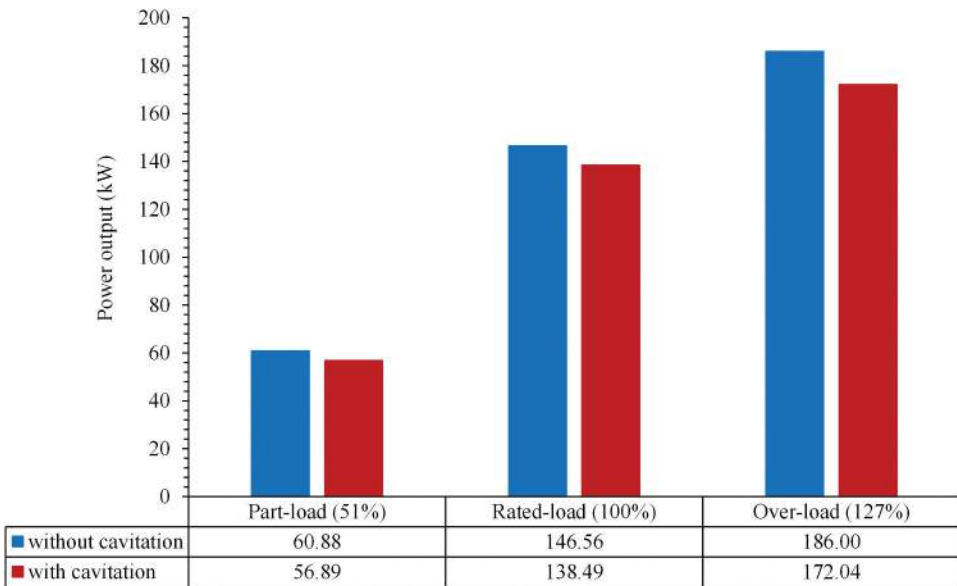


Figure 10. Power output with and without cavitation at different loading conditions.

leading edge of runner blade was observed at over-load condition, and the maximum pressure variations across trailing edge of runner blade was observed at part-load condition. The minimum pressure variations across runner blade was observed at rated-load condition.

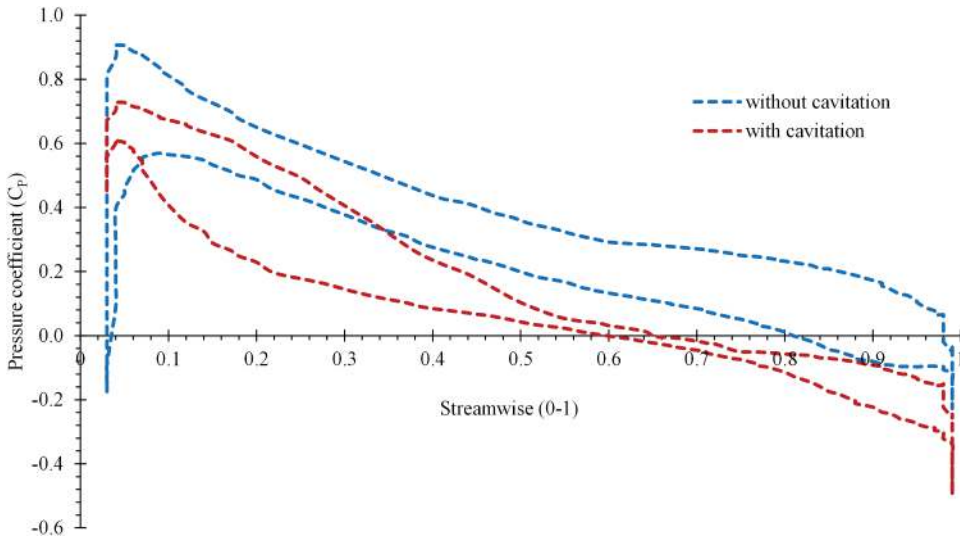


Figure 11. Pressure pulsation on runner blade surface under part-load condition.

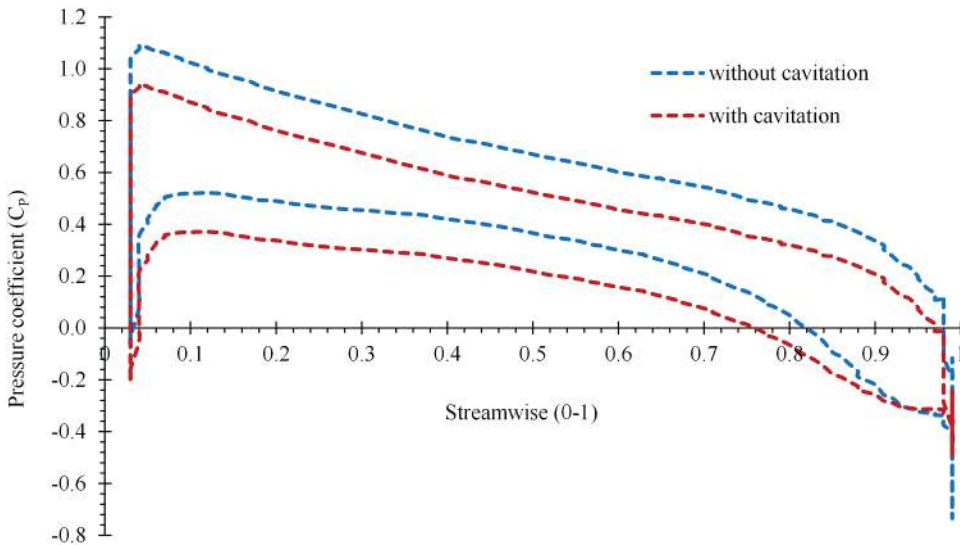


Figure 12. Pressure pulsation on runner blade surface at rated-load condition.

Cavitation characteristics of turbine

In order to derive the cavitation characteristics of considered turbine, a sigma curve has been plotted at different loading conditions and different stages of cavitation on the surface of blade has been discussed.

Sigma curve for turbine

The value of sigma (cavitation coefficient) for different values of draft tube outlet pressure has been calculated by using Equation (2). A value of critical sigma has also been computed from this curve at each loading conditions. In general, the point on sigma curve from where the value of hydraulic efficiency drops from initial value (value of hydraulic efficiency without cavitation) is known as critical

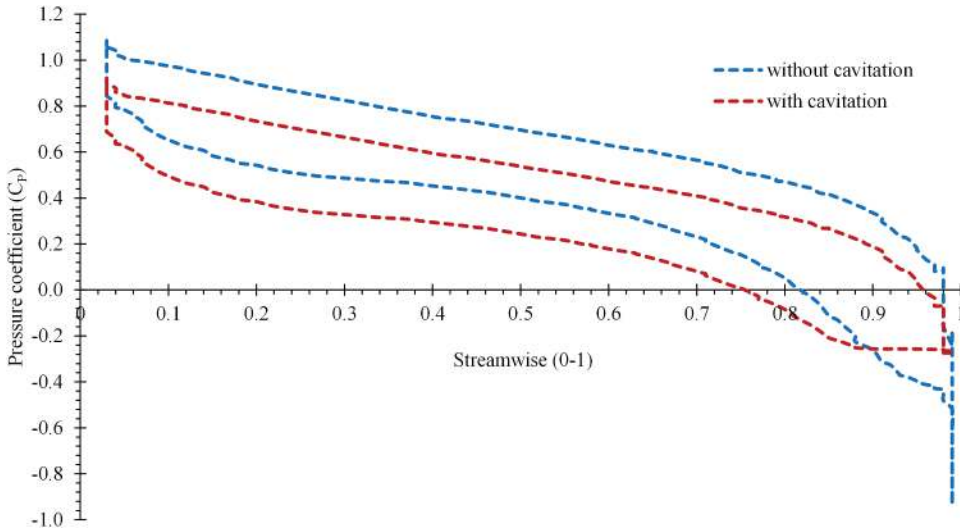


Figure 13. Pressure pulsation on runner blade surface during over-load condition.

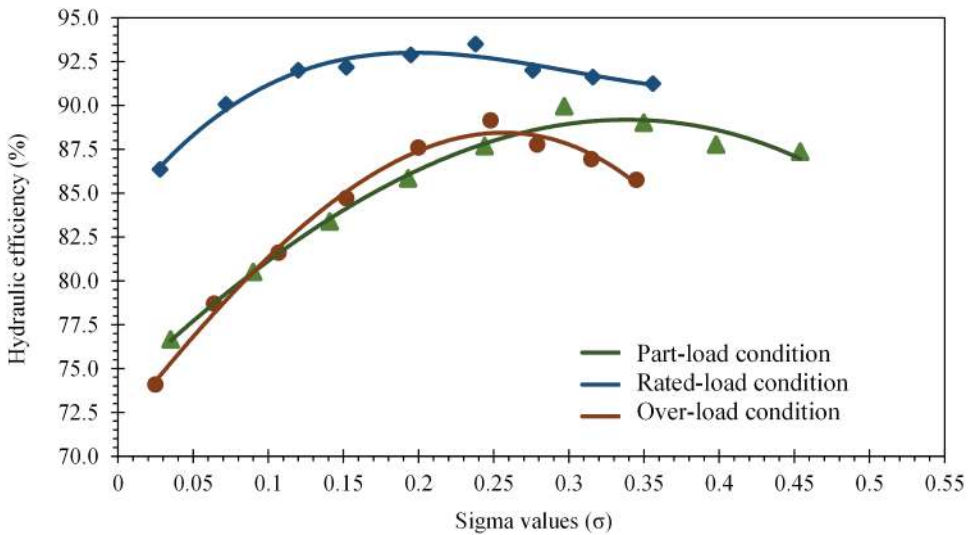


Figure 14. Sigma curve at different loading conditions.

sigma. In order to keep the turbine cavitation free operation, the sigma plant should be greater than the sigma critical. The sigma curve for part-load, rated-load, and over-load condition is shown in Figure 14.

Cavitation characteristics of Francis turbine model is described by ‘Sigma curve.’ This curve is obtained by changing the pressure condition at the outlet of draft tube, and it plays a significant role to determine the cavitation-free zone during operation of Francis turbine. As static pressure at outlet of draft tube decreases, the value of sigma will decrease. Initially, hydraulic efficiency increases due to reduction in ‘friction losses’ provided by collapsing bubble cavities. Further decrease in sigma value causes reduction in hydraulic efficiency of turbine due to obstruction to incoming water.

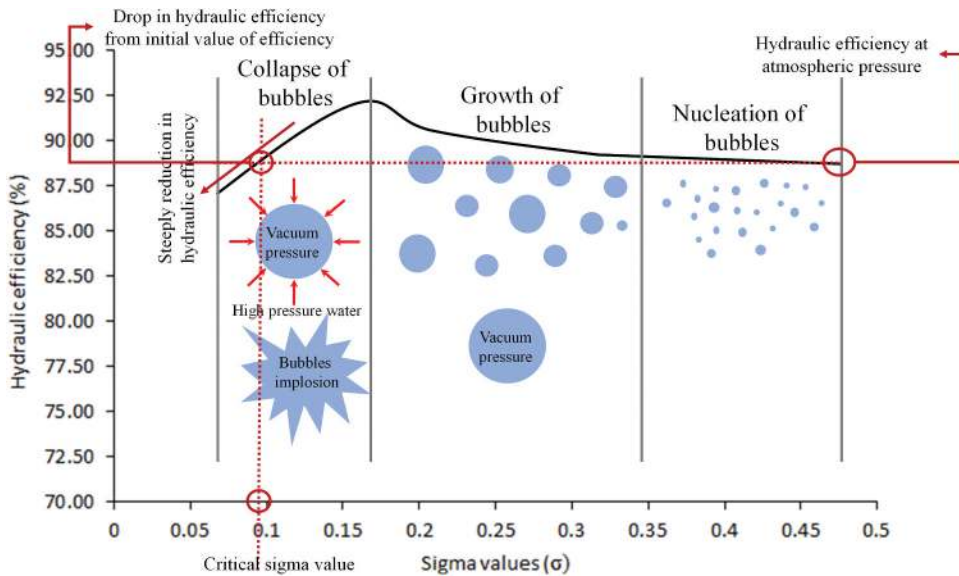


Figure 15. Schematics of cavitation phenomenon in hydro turbine (Avellan 2004).

The value of sigma at which hydraulic efficiency of hydro turbine will drop from its actual hydraulic efficiency is termed as 'Critical sigma.' The critical sigma has been calculated for all conditions in order to understand the range of cavitation-free operation. The graphical illustration for the determination of value of critical sigma is presented in Figure 15.

The value of critical sigma for part-load, rated-load, and over-load conditions were obtained as 0.18, 0.12, and 0.16, respectively. The minimum value of critical sigma is found corresponding to the rated-load of the turbine. However, the off-design conditions experience the larger value of critical sigma as compared to critical sigma value for rated-load condition. Based on this investigation, it is reported that turbine operating closer to critical sigma value shows that turbine can accommodate variable discharge conditions for a cavitation free operation of turbine. From Figure 16, it was concluded that the chances of inception of cavitation are more prominent at part-load regime than other loading regimes. Also, the critical sigma was found minimum at rated-load condition.

Progression of cavitation on blade surface

The development of cavitation on blade surface can be predicted by vapor volume fraction on the surface of runner blades. It defines the fraction of vapor distributed on blade surface. Its value varies from '0 to 1'. A '0' value indicates there is no water vapor around the blade surface, while '1' value indicates 100% water vapors. In this Francis turbine model, cavitation occurs mainly at the trailing edge of suction side and suction side of runner blade.

As the value of sigma decreases, more vapor bubbles were found to be accumulated around the surface of runner blade. As the flow leaves trailing edge of runner blade, a narrow wake zone is created, which is a low-pressure zone. At this location, the cavitation is more prone to occur. The stages of cavitation at different sigma values (different draft tube exit pressure) is shown in Figure 16. It is clearly seen that the cavitation reached its developed stage at a draft tube exit pressure of 0.6 atm. for over-load operation and 0.2 atm. for part-load and rated-load operation.

Flow variations in turbine runner

In order to obtain the transient hydrodynamic behavior of water flow across the Francis runner blades, the cavitation distribution in terms of Thoma cavitation number and inter-blade vortices distribution and velocity contours with streamline have been presented. To obtain the unsteadiness of flow around

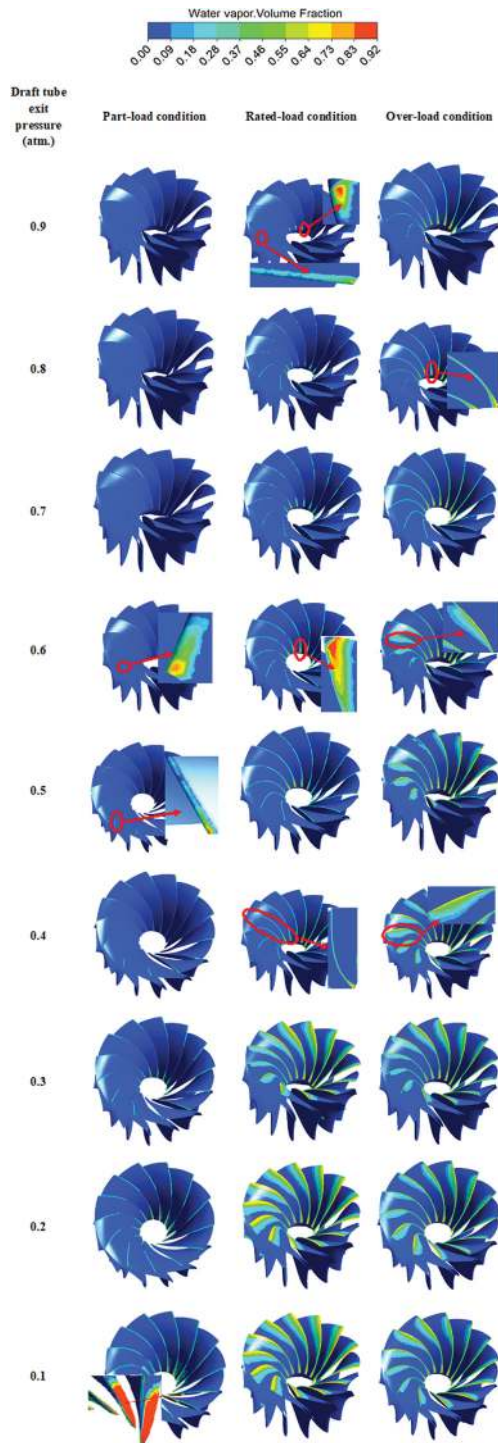


Figure 16. Vapor volume fraction at different draft tube exit pressure.

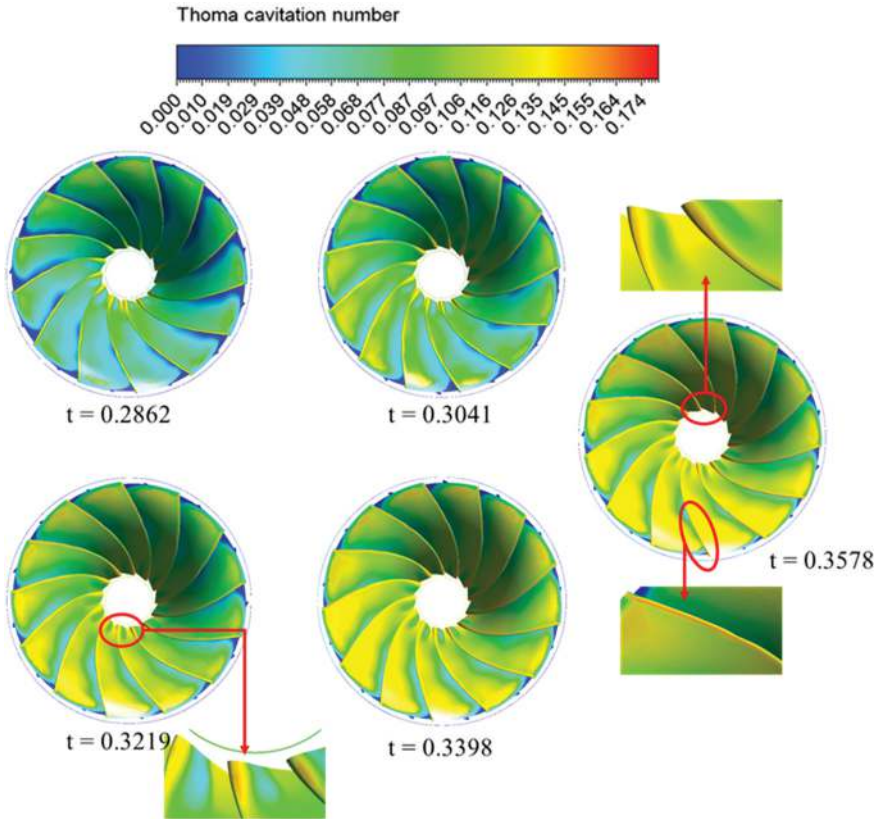


Figure 17. Distribution of Thoma's cavitation coefficient on the Francis runner blades.

runner blades under cavitation conditions, the contour has been plotted at every 90° angular position of turbine for a complete revolution. Hence, in total, five different angular positions of the turbine runner were considered.

Cavitation distributions on runner blades. To capture the pressure field variations across the turbine runner, the cavitation distributions corresponding to Francis runner on runner blades were obtained to effectively visualize the cavitation zone. The distributions of Thoma cavitation number on runner blades are shown in [Figure 17](#). The magnitude of cavitation from minimum to maximum is represented on a scale. It is observed that the trailing edge of runner blades is more prone to cavitation irrespective of runner angular position. It is due to the deceleration of flow from leading edge to trailing edge of blades. The cavitating zone on runner blades gets enlarged with the turbine rotation. It revealed that the detachment of flow at suction side of runner blades also complement this behavior. The developed stage of cavitation is obtained as the turbine completes its one cycle of revolution (at 360°).

An attempt has also been made to capture the inter-blade cavitating vortices at part-load conditions. On the same lines, Liu, Liu, and Zhao (2017) reported that the reduction of flow discharge in runner blades passage will cause high pulsating pressure around blades and leads to inter-blade vortex phenomenon. In order to capture inter-blade vortices in this turbine model, Q-criterion method was adopted by Lee, Lee, and Lim (2016), and Q-coefficient value was set as 0.261. In the present investigations, it is observed that as the runner start rotating, the vortices formed only at the trailing edge of runner blades (inception stage), but as it progresses, the vortices dominate and accumulate at the suction side of blade surface (developed stage) as shown in [Figure 18](#). In the present numerical

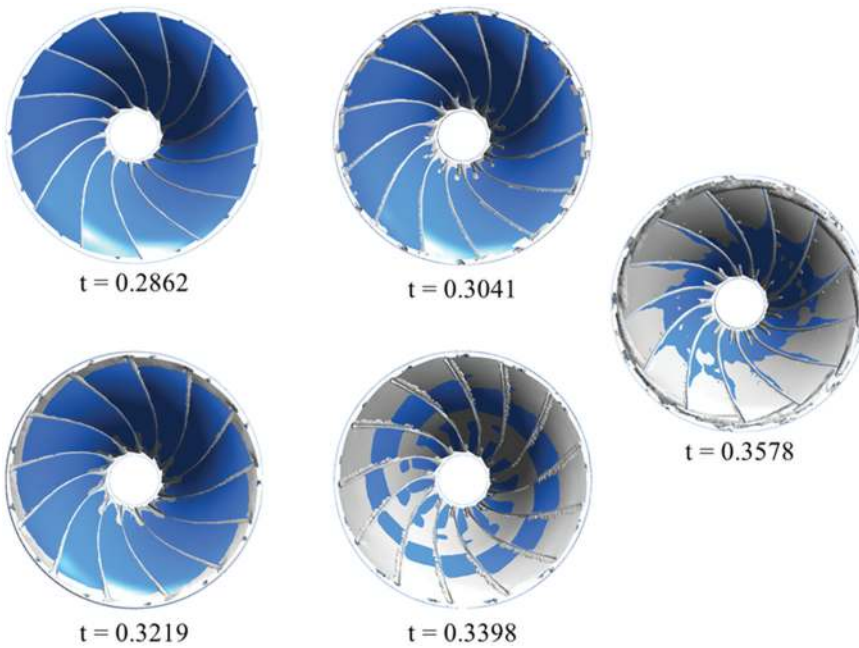


Figure 18. Unsteady behavior of Inter-blade vortices around runner blades.

investigation, the adopted numerical model has not reported the formation of vortex rope at the considered part load operating condition. However, to verify the generation of vortex rope for the considered turbine model, the experimental testing needs to be done to define the operating range for the formation of vortex rope. Further, it will also validate the non-formation of vortex rope in the considered part load condition adopted in the present study.

Velocity distribution on runner blades under cavitation condition. The velocity contour yield to development of flow velocity and its variations across the turbine rotor. To numerically investigate the velocity in stationary frame has been plotted on X-Y plane under cavitation condition to observe the transient behavior of water around guide vane and runner blades. In order to observe the nature of flow around runner blades, one of the runner blades has been marked with violet color point, and this point was observed on blade over one cycle of revolution. In present study, total five number of revolutions of Francis runner was considered to achieve the periodic steady-state behavior. Moreover, last revolution of Francis runner is accounted for to plot contours of velocity along with streamlines. In this view, runner starts rotating at $\theta = 0^\circ/t = 0.2862s$ (last time step of fourth revolution), and at $\theta = 360^\circ/t = 0.0.3578s$, runner will complete the last or 5th revolution. The streamlines were incorporated on velocity contour to visualize the vortex formation around the runner blades. Smooth flow is found toward runner from guide vanes while recirculations are observed from suction side of runner blades due to curvature of runner blades. The velocity distribution along the flow domain with streamlines at various rotation angles is shown in [Figure 19](#).

Based on flow visualization, it is found that the unsteadiness in flow domain significantly affect the local cavitation characteristics of medium speed Francis runner. It is observed that as rotation progresses, the sigma value starts from minimum level and vapor bubbles accumulate at the trailing edge of runner blades (inception stage). However, the more bubbles are generated on the suction side of runner blades and attain the developed stage of cavitation at the end of rotation ([Figure 17](#)). It signifies that the rotational motion of Francis runner causes local pressure drop on the suction side

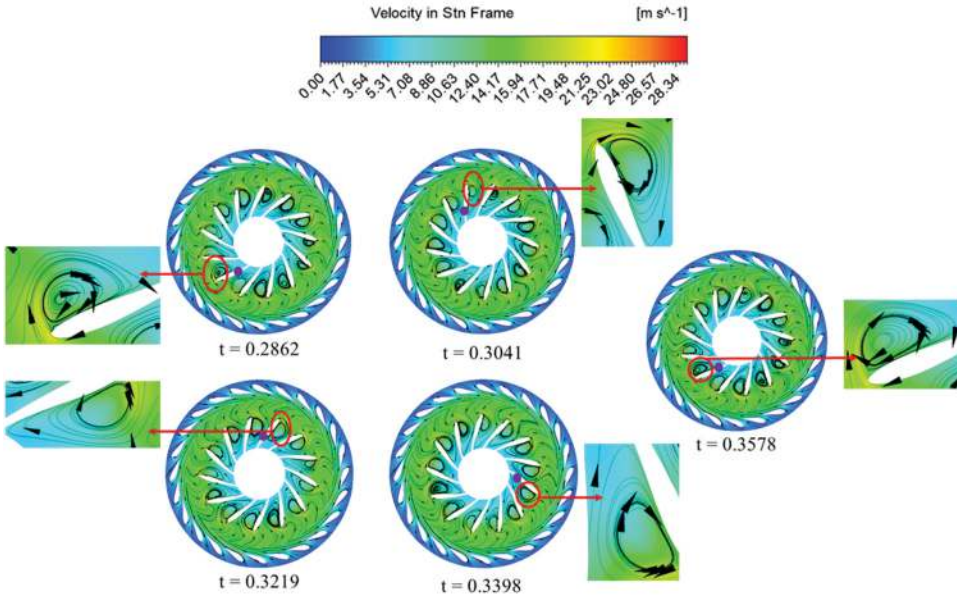


Figure 19. Velocity distribution along with streamlines at various rotation angles.

along with trailing edge of runner blades. The unsteadiness also affects the generation of inter-blade vortices in Francis runner as shown in Figure 18. Therefore, the runner rotation leads to generation of inter-blade vortices on the blade area near to shroud.

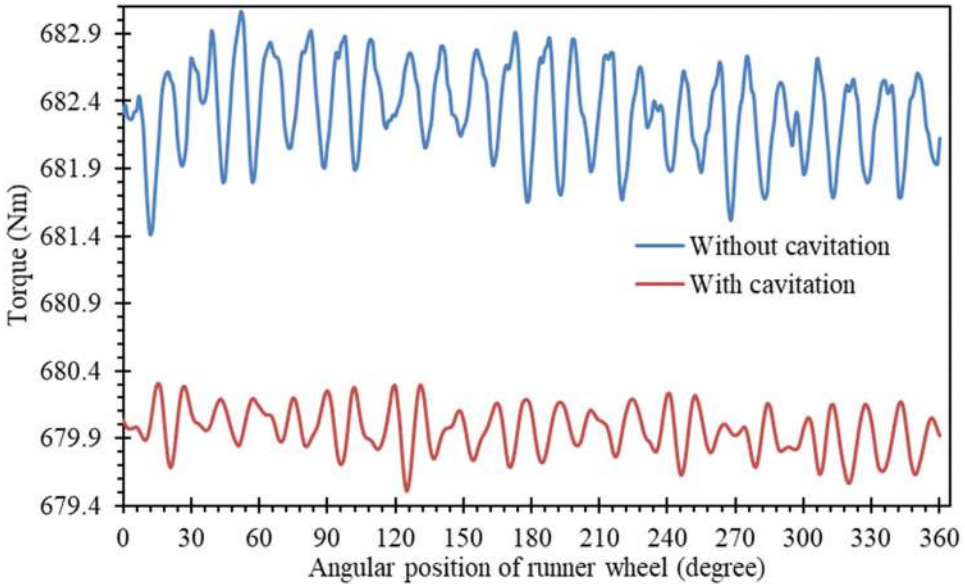


Figure 20. Variation of torque developed by turbine runner with and without cavitation conditions.

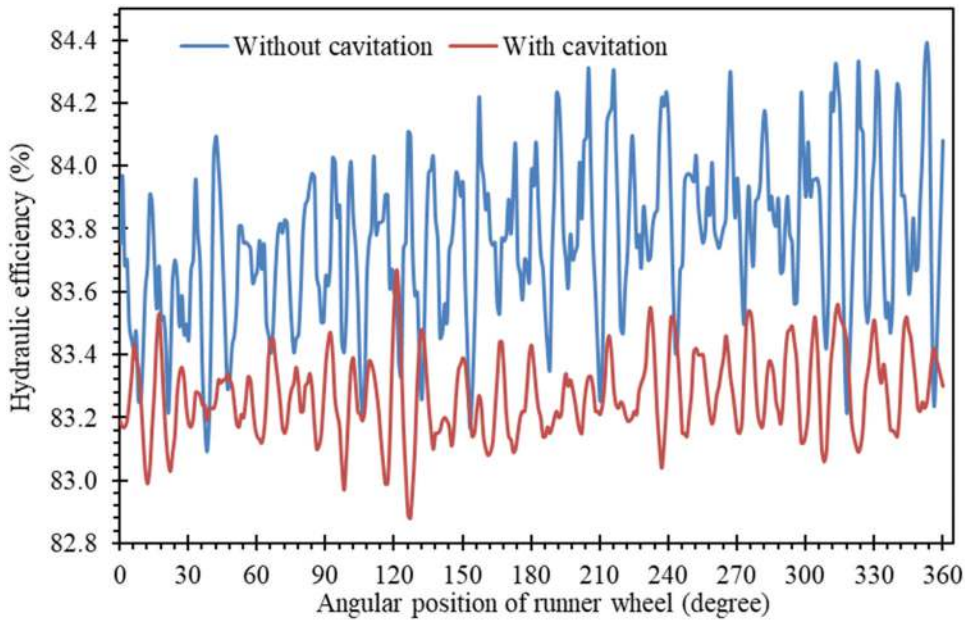


Figure 21. Variation in hydraulic efficiency of turbine runner with and without cavitation conditions.

Assessment of performance parameters under cavitation and without cavitation conditions

As discussed in the earlier sections, cavitation phenomena is more severe in part-load operation as compared to rated and overload conditions. Therefore, unsteady assessment has also been made to evaluate and compare the turbine performance with cavitation ($\sigma = 0.18$) and without cavitation conditions in terms of hydraulic efficiency and torque developed by the turbine runner at part-load regime. The study revealed that turbine rotor torque (mean) is found to be reduced by 0.404% under cavitation condition as compared to runner torque under without cavitation regimes. This phenomenon also impacted the hydraulic efficiency of turbine, and a drop of about 0.86% was observed corresponding to cavitation regime. The reduction in the runner torque and hydraulic efficiency were caused by insufficient interaction of water with runner blades due to presence of water bubbles, which were generated by the density difference between water bubbles and water. The insufficient interaction of water with runner blades significantly reduced the reactive force generated by runner blades and hence the torque under cavitation condition. The variation of torque and hydraulic efficiency with and without cavitation conditions are presented in [Figures 20 and 21](#), respectively.

Conclusions

The present study deals with the performance and cavitating flow analysis of the Francis turbine runner under different load regimes. The numerical simulations were performed with steady and transient approach, and the results were validated with the model testing. Hydraulic efficiency, power output, and net head were monitored under part-load, rated load, and over-load conditions. Based on the results, it has been concluded that loss in hydraulic efficiency, net head, and power output was minimum corresponding to rated load, and maximum difference was found during overload operation under cavitating flow conditions. The overload operation of the turbine results in the maximum difference in the turbine efficiency, and as the operation of the turbine shift toward rated load conditions, turbine start to regain its best efficiency point. Cavitation phenomenon was evaluated by generating the sigma curve for the considered loading regimes, and it has been concluded that

reduction in friction losses increases the turbine efficiency, which is caused due to formation of small bubble cavities during the inception stage of cavitation. The values of critical sigma were computed as 0.18, 0.12, and 0.16 corresponding to part-load, rated-load, and over-load conditions, respectively. The maximum value of critical sigma was obtained corresponding to part-load condition, which signifies that inception of cavitation occurs earlier to part-load regime than other considered loading regimes. The quantum of vapor bubbles was found to be more in the over-load operating conditions. Under part-load operation regime for cavitation conditions, the Thoma cavitation number is found to increase as runner blades rotate. The inter-blade cavitating vortices also been captured at part-load operating condition. The formation of recirculating flow has also been observed at the suction side of runner blades at each rotor angle. Under cavitation condition, the torque and hydraulic efficiency of turbine runner were found to be reduced by 0.404% and 0.86%, respectively. Based on the investigations, it is observed that the part-load operation of the turbine requires a careful operation to prevent the turbine from severe damages to the turbine runner in comparison to turbine operation under other considered loading regimes (Full load and overload). The results of the present study will be useful for the design, operation, and maintenance of medium-specific speed turbines. Further, investigations will be carried out for the material selection and design optimization to overcome the problem associated with the part-load operation of the turbine, which further may reduce the chances of cavitation phenomena.

Nomenclature

η_H	Hydraulic efficiency (%)	ω	Angular speed of runner (rad/s)
P_o	Power output (watt)	Q	Flow discharge (m^3/s)
P_i	Power input (watt)	P_{inlet}	Total inlet pressure (Pa)
T	Torque developed by runner (N-m)	P_{outlet}	Total outlet pressure (Pa)
σ_{plant}	Plant cavitation number	σ_{turb}	Turbine cavitation number
P_a/p_∞	Ambient pressure (Pa)	P_v	Vapor pressure (Pa)
P_i	Absolute pressure of water at any point in flow domain (Pa)	P_2	Total pressure at the outlet of runner (Pa)
W_2	Relative velocity at the outlet of runner (m/s)	t	Time step size (second)
H_s	Suction head (m)	H	Net head across turbine (m)
kW	Kilo-watt	MW	Mega-watt
GVA	Guide vane angle ($^\circ$)	K	Turbulent kinetic energy
μ_t	Turbulent viscosity (Pa.s)	S	Invariant measure of the strain rate (s^{-1})
f_2	Blending function	\dot{m}_v'	Mass transfer rate of vaporization(kg/s)
\dot{m}_c'	Mass transfer rate of condensation (kg/s)	p_B	Pressure inside vapour bubbles (Pa)
R	Mean radius of bubble (m)	ρ_l	Density of liquid (kg/m^3)
α	Guide vane angle ($^\circ$)	OP	Operating points
N_{11}	Unit speed of turbine (rpm)	Q_{11}	Specific flow rate (litre/s)

Disclosure statement

No potential conflict of interest was reported by the author(s).

Notes on contributors

Md. Mustafa Kamal is pursuing Ph.D. from the Department of Hydro and Renewable Energy at IIT Roorkee, Roorkee, India. His work mainly focuses on hydro turbines and hydrokinetic turbines. He received his Masters from Maulana Azad National Institute of Technology, Bhopal, India in the field of hydropower engineering.

Dr. Gaurav Saini is presently working as Assistant Professor in the School of Advanced Materials, Green Energy and Sensor Systems, Indian Institute of Engineering Science and Technology (IEST) Shibpur India. He received his Ph.D. in Renewable Energy (Hydrokinetic Turbines) in the year 2020 and M. Tech, (Fluid Machinery and Energy Systems) in the year 2014 from Indian Institute of Technology Roorkee, Uttarakhand India. His research areas include Renewable Energy (Hydrokinetic Energy, Wind Power, and Biomass), Computational Fluid Dynamics (CFD), and Fluid Mechanics

and Fluid Power. Dr. Saini is skilled in Computational Fluid Dynamics (CFD) - numerical modeling and roto-dynamics analysis, Multiphase flow analysis, Modeling of various renewable energy resources viz. wind, marine, solar and hydrokinetic energy for rural applications, wind and hydrokinetic- Technology selection and design, Installation strategies, Performance evaluation, and O&M issues.

Dr. Ali Abbas earned his Ph.D. from the Department of Hydro and Renewable Energy at IIT Roorkee, Roorkee, India. His work mainly focuses on the transient phenomena in the draft tubes of hydro turbines. He is currently working at Flovel Energy Pvt. Ltd., Faridabad, India, as a manager – Design and Engineering.

Dr. Vishnu Prasad is a Professor in the Department of Civil Engineering at Maulana Azad National Institute of Technology, Bhopal, India. He earned his Ph.D. in the field of hydropower. His work mainly focuses on fluid mechanics, hydropower, and CFD.

ORCID

Gaurav Saini  <http://orcid.org/0000-0001-9593-5180>

References

- Avellan, F., 2004. Introduction to cavitation in hydraulic machinery. 6th Int. Conf. Hydraul. Mach. Hydrodyn October 21-22, 2004. Timisoara: Politehnica University of Timișoara. Timisoara, Romania. 11–22.
- Blazek, J. 2001. *Computation fluid dynamics: Principles and applications*, 3, Iddington, Oxford OX5 1GB. UK: Elsevier , 228–40. 978-0-08-044506-9. <https://doi.org/10.1016/B978-0-08-044506-9.X5000-0>
- Celebioglu, K., B. Altintas, S. Aradag, and Y. Tascioglu. 2017. Numerical research of cavitation on Francis turbine runners. *International Journal of Hydrogen Energy* 42 (28):17771–81. doi:10.1016/j.ijhydene.2017.03.180.
- Celebioglu, K., S. Aradag, E. Ayli, and B. Altintas. 2018. Rehabilitation of Francis turbines of power plants with computational methods. *Hittite Journal of Science & Engineering* 5 (1):37–48. doi:10.17350/HJSE19030000076.
- Chang, H., X. Xie, Y. Zheng, and S. Shu. 2017. Numerical study on the cavitating flow in liquid hydrogen through elbow pipes with a simplified cavitation model. *International Journal of Hydrogen Energy* 42 (29):18325–32. doi:10.1016/j.ijhydene.2017.04.132.
- Chirkov, D. V., S. G. Cherny, P. K. Shcherbakov, V. A. Skorospelov, and A. V. Zakharov. 2019. -dimensional simulation of full load instability in Francis turbines. *Journal of Hydraulic Research* 57 (5):623–34. doi:10.1080/00221686.2018.1494047.
- Decaix, J., A. Muller, F. Avellan, and C. Munch. 2015. RANS computations of a cavitating vortex rope at full load, 6th IAHR International Meeting of the Workgroup on Cavitation and Dynamic Problems in Hydraulic Machinery and Systems, September 9-11, 2015, Ljubljana, Slovenia.
- Ghahramani, E., M. H. Arabnejad, and R. E. Bensow. 2019. International Journal of Multiphase Flow A comparative study between numerical methods in simulation of cavitating bubbles. *International Journal of Multiphase Flow* 111:339–59. doi:10.1016/j.ijmultiphaseflow.2018.10.010.
- Gohil, P. P., and R. P. Saini. 2015. Effect of temperature, suction head and flow velocity on cavitation in a Francis turbine of small hydro power plant. *Energy* 93:613–24. doi:10.1016/j.energy.2015.09.042.
- Gohil, P. P., and R. P. Saini. 2016. Numerical study of cavitation in Francis turbine of a small hydro power plant. *Journal of Applied Fluid Mechanics* 9 (1):357–65. doi:10.18869/acadpub.jafm.68.224.24080.
- Huang, B., Q. Wu, and G. Wang. 2014. Numerical investigation of cavitating flow in liquid hydrogen. *International Journal of Hydrogen Energy* 39 (4):1698–709. doi:10.1016/j.ijhydene.2013.11.025.
- IHA. 2020. Hydropower status report 2020. *International Hydropower Association* 1–83. doi:10.1103/PhysRevLett.111.027403.
- Jain, A. K. 2002. *Fluid mechanics and hydraulic machines*. New Delhi: KHANNA PUBLISHERS, 835–36. ISBN: 978-8174091949 .
- Jean, P. F., and M. M. Jean. 2004a. Nuclei and Cavitation. *Fundamentals of cavitation*, 1st edition, 76. Fluid Mechanics and Its Applications. France: Springer Dordrecht .Chapter-1, XXII, 306, 978-90-481-6618-3. <https://doi.org/10.1007/1-4020-2233-2> .
- Jean, P. F., and M. M. Jean. 2004b. The Dynamics of Spherical Bubbles . *Fundamentals of cavitation*, 1st edition, 76. Fluid Mechanics and Its Applications. France: Springer Dordrecht . Chapter-1, XXII, 306. doi:10.1007/1-4020-2233-6_3.
- Kamal, M., A. Abbas, V. Prasad, and R. Kumar. 2021. A numerical study on the performance characteristics of low head Francis turbine with different turbulence models. *Materials Today: Proceedings*. doi:10.1016/j.matpr.2021.02.155.
- Kamal, M. 2017. Scenario of small hydro power projects in India and its environmental aspect. *International Research Journal of Engineering and Technology* 4:228–34.
- Lal, J. 2011. *Hydraulic machines*. Delhi: Metropolitan Book Co. Pvt. Ltd.

- Laouari, A., and A. Ghenaïet. 2016. Simulations of steady cavitating flow in a small Francis turbine. *International Journal of Rotating Machinery* 2016:1–15. Article ID 4851454. doi:10.1155/2016/4851454.
- Lee, J. H., Y. T. Lee, and H. C. Lim. 2016. Effect of twist angle on the performance of Savonius wind turbine. *Renewable Energy* 89:231–44. doi:10.1016/j.renene.2015.12.012.
- Liu, D., X. Liu, and Y. Zhao. 2017. Experimental investigation of inter-blade vortices in a model Francis turbine. *Chinese Journal of Mechanical Engineering* 30 (4):854–65. doi:10.1007/s10033-017-0097-1.
- Liu, X., Y. Luo, B. W. Karney, and W. Wang. 2015. A selected literature review of efficiency improvements in hydraulic turbines. *Renewable and Sustainable Energy Reviews* 51:18–28. doi:10.1016/j.rser.2015.06.023.
- Menter, F. R. 1994. Two-Equation Eddy-Viscosity turbulence models for engineering applications. *AIAA Journal* 32 (8):1598–605. doi:10.2514/3.12149.
- Ramirez, C., A. Leroyer, E. Guilmineau, P. Queutey, and E. C. Nantes. 2003. Numerical features of cavitation models based on the simplified Rayleigh-Plesset equation 19th Numerical Towing Tank Symposium (NuTTS 2016), Oct., 2016, St. Pierre d’Oleron, France: 114–119.
- Saini, G., and R. P. Saini. 2019. A review on technology, configurations, and performance of cross-flow hydrokinetic turbines. *Journal of Energy Research* 43:6639–79.
- Saini, G., and R. P. Saini. 2020a. A computational investigation to analyze the effects of different rotor parameters on hybrid hydrokinetic turbine performance. *Ocean Engineering* 199:107019. doi:10.1016/j.oceaneng.2020.107019.
- Saini, G., and R. P. Saini. 2020b. Comparative investigations for performance and self-starting characteristics of hybrid and single Darrieus hydrokinetic turbine. *Energy Reports* 6 (2):96–100. doi:10.1016/j.egy.2019.11.047.
- Su, W. T., X. B. Li, F. C. Li, W. F. Han, X. Z. Wei, and J. Guo. 2013. Large eddy simulation of pressure fluctuations at off-design condition in a Francis turbine based on cavitation model, 6th International Conference on Pumps and Fans with Compressors and Wind Turbines, 19–22 September 2013. Beijing, China, 52, IOP Conf. Series: Materials Science and Engineering, 022032. doi:10.1088/1757-899X/52/2/022032 .
- Sun, L., P. Guo, and X. Luo. 2020. Numerical investigation on inter-blade cavitation vortex in a Francis turbine. *Renewable Energy* 158:64–74. doi:10.1016/j.renene.2020.05.034.
- Tiwari, G., J. Kumar, V. Prasad, and V. Kumar. 2020b. Derivation of cavitation characteristics of a 3MW prototype Francis turbine through numerical hydrodynamic analysis. *Materials Today: Proceedings* 26:1439–48. doi:10.1016/j.matpr.2020.02.297.
- Trivedi, C., B. Gandhi, and C. J. Michel. 2013. Effect of transients on Francis turbine runner life A review. *Journal of Hydraulic Research* 51 (2):121–32. doi:10.1080/00221686.2012.732971.
- Trivedi, C., I. Iliev, O. G. Dahlhaug, Z. Markov, F. Engstrom, and H. Lysaker. 2020. Investigation of a Francis turbine during speed variation: Inception of cavitation. *Renewable Energy* 166:147–62. doi:10.1016/j.renene.2020.11.108.
- Versteeg, H. K., and W. Malalasekera. 2007. Conservation laws of fluid motion and boundary conditions . *An introduction to computational fluid dynamics 2* (USA: Pearson) . Chapter 2, 21: 978-0-13-127498-3 .
- Wack J and Riedelbauch S. (2017). Numerical simulation of a cavitating draft tube vortex rope in a Francis turbine at part load conditions for different σ -levels. *J. Phys.: Conf. Ser.*, 813: 012019. doi:10.1088/1742-6596/813/1/012019
- Wack, J., S. Riedelbauch, W. Kreider, A. Maxwell, B. Cunitz, and M. Bailey. 2015. Numerical simulations of the cavitation phenomena in a Francis turbine at deep part load conditions. *Journal of Physics. Conference Series* 656. doi:10.1088/1742-6596/656/1/012027.
- Wei, X. Z., W. T. Su, X. B. Li, F. C. Li, and L. Guo. 2014. Effect of blade perforation on Francis hydro-turbine cavitation characteristics. *Journal of Hydraulic Research* 52 (3):412–20. doi:10.1080/00221686.2013.879610.
- Yamamoto, K., A. Müller, A. Favrel, and F. Avellan Nov. 2019. Physical mechanism of interblade vortex development at deep part load operation of a Francis turbine. *Journal of Fluids Engineering, Transactions of the ASME* 141 11 111113 doi:10.1115/1.4043989.
- Yang, J., L. J. Zhou, and Z. W. Wang. 2019. Numerical investigation of the cavitation dynamic parameters in a Francis turbine draft tube with columnar vortex rope. *Journal of Hydrodynamics*, 31(5):931–39. doi:10.1007/s42241-019-0035-z.
- Yu, A., X. W. Luo, and B. Ji 2015. Numerical simulation and analysis of the internal flow in a Francis turbine with air admission, International Symposium of Cavitation and Multiphase Flow (ISCM 2014), Oct. 18-24, 2014. Beijing, China, 72 (IOP Conference Series Materials Science and Engineering)042047. doi:10.1088/1757-899X/72/4/042047 .
- Zhang, Y., K. Liu, H. Xian, and X. Du. 2018. A review of methods for vortex identification in Hydro turbines. *Renewable and Sustainable Energy Reviews* 81:1269–85. July 2017. doi:10.1016/j.rser.2017.05.058.
- Zhang, Z., Z. Yu, H. Gao, N. Cheng, and J. Wang. 2019. Research on the cavitation characteristic improvement of impellers of HL220 turbine. *Environmental Earth Sciences* 78 (12):1–9. doi:10.1007/s12665-019-8361-6.